Developmental Biology 385 (2014) 304–315

Contents lists available at ScienceDirect

Developmental Biology

journal homepage: www.elsevier.com/locate/developmentalbiology

A comparative study of nucleostemin family members in zebrafish reveals specific roles in ribosome biogenesis

Paul B. Essers [a], Tamara C. Pereboom [a], Yvonne J. Goos [a], Judith T. Paridaen [b], Alyson W. MacInnes [a,*]

[a] Hubrecht Institute, KNAW and University Medical Center Utrecht, Uppsalalaan 8, 3584CT Utrecht, The Netherlands
[b] Max-Planck-Institute of Molecular Cell Biology and Genetics, Pfotenhauerstrasse 108, D-01307 Dresden, Germany

ARTICLE INFO

Article history:
Received 10 June 2013
Received in revised form
24 October 2013
Accepted 28 October 2013
Available online 6 November 2013

Keywords:
Nucleostemin
Ribosome biogenesis
p53

ABSTRACT

Nucleostemin (NS) is an essential protein for the growth and viability of developmental stem cells. Its functions are multi-faceted, including important roles in ribosome biogenesis and in the p53-induced apoptosis pathway. While NS has been well studied, the functions of its family members GNL2 and GNL3-like (GNL3L) remain relatively obscure despite a high degree of sequence and domain homology. Here, we use zebrafish lines carrying mutations in the *ns* family to compare and contrast their functions in vertebrates. We find the loss of zebrafish *ns* or *gnl2* has a major impact on 60S large ribosomal subunit formation and/or function due to cleavage impairments at distinct sites of pre-rRNA transcript. In both cases this leads to a reduction of total protein synthesis. In contrast, *gnl3l* loss shows relatively minor rRNA processing delays that ultimately have no appreciable effects on ribosome biogenesis or protein synthesis. However, the loss of *gnl3l* still results in p53 stabilization, apoptosis, and lethality similarly to *ns* and *gnl2* loss. The depletion of p53 in all three of the mutants led to partial rescues of the morphological phenotypes and surprisingly, a rescue of the 60S subunit collapse in the ns mutants. We show that this rescue is due to an unexpected effect of p53 loss that even in wild type embryos results in an increase of 60S subunits. Our study presents an in-depth description of the mechanisms through which *ns* and *gnl2* function in vertebrate ribosome biogenesis and shows that despite the high degree of sequence and domain homology, *gnl3l* has critical functions in development that are unrelated to the ribosome.

Introduction

Nucleostemin (NS or GNL3) is a protein critical for development via its function in the growth and maintenance of stem cells. The initial studies of NS showed that while its expression is very high in stem and cancer cells, this expression rapidly declined as cells proceeded towards terminal differentiation (Tsai and McKay, 2002). Conversely, ns (or Ns) expression has been shown to accumulate in de-differentiating cells of regenerating newt limbs and murine hepatocytes after severe liver injury, suggesting it plays an important role in tissue regeneration (Maki et al., 2007; Shugo et al., 2012). Recently it has also been shown that the self-renewal of stem cells requires functional Ns in murine blastocytes to facilitate a rapid transition through G1 phase of the cell cycle (Qu and Bishop, 2012). Yet despite the unquestionable importance of NS in development and stem cell maintenance, the exact functions of NS remain incompletely understood.

NS has two family members, GNL2 (or Ngp-1) and GNL3-like (GNL3L), that all contain a MMR_HSR1 domain described by five GTP-binding motifs arranged in a circularly permuted order (Meng et al., 2007). *GNL3L* is the vertebrate paralogue of *NS*, the two sharing the common *Grnlp* orthologue in yeast and the highest level of sequence similarity in vertebrates, while *GNL2* remains a single gene in both vertebrates and invertebrates. In all three proteins the binding of GTP to their common motifs controls the shuttling of the proteins from the nucleus to the nucleolus, the organelle where the majority of ribosome biogenesis takes place (Tsai and McKay, 2005). This observation led to a number of studies focusing on a potential function of NS in synthesis of the ribosome. Co-immunoprecipitation studies show that NS forms a complex with several ribosomal proteins and factors involved in ribosomal RNA (rRNA) processing, although NS is not itself part of the ribosome The knockdown of ns in *Drosophila melanogaster* results in failure of the nucleolus to release 60S ribosomal subunits (Romanova et al., 2009a, 2009b; Rosby et al., 2009), and the knockdown of human NS in HeLa cells followed by pulse-chase

* Corresponding author. Fax: +31 30 2516 464.
E-mail addresses: p.essers@hubrecht.eu (P.B. Essers), t.pereboom@hubrecht.eu (T.C. Pereboom), y.goos@hubrecht.eu (Y.J. Goos), paridaen@mpi-cbg.de (J.T. Paridaen), a.macinnes@hubrecht.eu (A.W. MacInnes).

0012-1606/$ - see front matter © 2013 Elsevier Inc. All rights reserved.
http://dx.doi.org/10.1016/j.ydbio.2013.10.029

experiments suggests this involves delayed processing of 32S to 28S rRNA (Romanova et al., 2009a). However, the precise role of NS and how it functions to process pre-rRNA into mature rRNA is still unknown, and a specific ribosomal function for GNL2 or GNL3L in vertebrates has not been reported to date.

NS also has an established role in the p53 tumor suppressor pathway. The initial functional analysis of NS revealed that its overexpression prevents cells from entering mitosis and induces apoptosis in a p53-dependent manner (Tsai and McKay, 2002). It was later reported that overexpression of NS is able to stabilize the p53 tumor suppressor protein by directly binding to MDM2 and dissociating p53 in a manner dependent on the nucleoplasmic mobilization of NS (Dai et al., 2008). Conversely, depletion of NS has been demonstrated to activate p53 by the nucleolar release of ribosomal proteins L11 and L5 that bind to MDM2, resulting in the dissociation of the p53/MDM2 complex and activation of p53 (Dai et al., 2008). GNL3L has also been reported to bind to and stabilize MDM2 *in vivo* while its depletion results in p53-dependent G2/M arrest, however unlike NS the interaction with MDM2 does not appear to be dependent on protein localization (Meng et al., 2011a).

Other lines of evidence also suggest that despite the homologies of the vertebrate NS family members they have evolved to perform independent functions. For example, the expression of murine Gnl3l is lower in undifferentiated vs. differentiated neural stem cells in stark contrast to Ns expression (Yasumoto et al., 2007). Moreover, in adult murine tissues Gnl3l is found expressed in the cerebellum and forebrain, while the expression of Ns is limited to the testis (Ohmura et al., 2008). In the developing zebrafish embryo, early expression (1 day post fertilization [dpf]) of *ns* is more restricted in the brain compared to *gnl2* and *gnl3l*, while only *gnl3l* shows strong expression in the tail (Paridaen et al., 2011; Thisse and Thisse, 2004). Protein interaction and cellular localization in mammalian studies also suggest divergent functions of human NS and GNL3L. NS binds not only to MDM2 and p53 but also ARF (alternate reading frame) and RSL1D1 (ribosomal L1 domain containing 1) (Dai et al., 2008; Ma and Pederson, 2007; Meng et al., 2006). GNL3L has also been shown to bind MDM2, as well as TERT (telomerase reverse transcriptase) and ERR (estrogen related receptor) protein (Fu and Collins, 2007; Meng et al., 2011a, 2006). Both NS and GNL3L bind to TRF1 and exert opposite effects, resulting in TRF1 degradation or stabilization, respectively (Meng et al., 2011b). In terms of localization, human NS is predominantly localized in the nucleolus while GNL3L is found mostly in the nucleoplasm and displays a shorter nucleolar retention time than does NS (Rao et al., 2006). No protein interaction studies or localization studies of GNL2 in any species have been done to date.

Our previous work demonstrated that the loss of Ns or Gnl2 protein in zebrafish results in incomplete retinal neurogenesis due to a failure of these cells to exit the cell cycle properly, consistent with previous *in vitro* and *in vivo* murine studies showing knockdown of Ns leads to G1-S phase arrest and reduced cell proliferation (Beekman et al., 2006b; Paridaen et al., 2011; Tsai and McKay, 2002). Zebrafish Ns and Gnl2 proteins have some degree of overlapping functions. We showed that expressing *ns* mRNA in *gnl2* mutants, and vice versa, was able to partially rescue the small head, small eye, and hindbrain ventricle inflation phenotypes that are characteristic of most ribosome biogenesis mutants in zebrafish embryos (Amsterdam et al., 1999; Paridaen et al., 2011). Moreover, the loss of both Ns and Gnl2 revealed a synergy of these phenotypes that was more substantial than the loss of either protein alone. The *ns* and *gnl2* mutants also revealed an increase in p53 stabilization, the expression of p53 target genes, and apoptosis; particularly in areas of robust proliferation such as the head and eye regions (Paridaen et al., 2011). However, expressing a loss-of-function *p53* gene or depleting p53 with morpholinos in mutant embryos did not rescue the retina phenotype or the lethality to any significant degree (Paridaen et al., 2011). This was in line with murine studies that showed no rescue effect of mutant *p53* expression on the lethal phenotype induced by the deletion of *Ns* (Beekman et al., 2006a). These data together suggested the relevance of p53-induced apoptosis upon Ns or Gnl2 loss is minor, and that other pathways contribute to the overall phenotypes. In our previous zebrafish study however, we did not examine the effects of Ns or Gnl2 loss on ribosome biogenesis.

As mentioned above, the deletion of *Ns* in mice is known to result in embryonic lethality at e.4 due to the failure of blastocysts to enter S-phase (Beekman et al., 2006a). However, the early lethality of these *Ns*(−/−) cells renders it challenging to perform experimental assays that require large numbers of cells, such as polysome profiling. In contrast, given the high fecundity and *ex utero* fertilization of zebrafish embryos we are able to collect unrestricted numbers of cells for assays that test how the loss of each *ns* family member affects various aspects of ribosome biogenesis despite the lethal phenotype. Given our previous results showing the overlapping functions of Ns and Gnl2, coupled to the high degree of homology of Gnl3l with Ns, we sought to determine in a vertebrate model if all three of the family members function similarly with respect to ribosome biogenesis and protein translation.

Materials and methods

Zebrafish mutant lines

Zebrafish embryos were raised and staged as previously described (Westerfield, 1995) in accordance with all Dutch regulations and guidelines under DEC protocol #08.2011. The *gnl2*^{bw41c} mutation was recovered in a forward genetic screen, whereas the *ns*^{hu3259} mutation was generated in a reverse genetic screen using the TILLING method (Wienholds and Plasterk, 2004). The *gnl3l* mutant was uncovered in a viral insertion mutagenesis screen (Golling et al., 2002). Mutants were identified by their morphological phenotypes including reduced body size, smaller heads and eyes, and inflation of the hindbrain ventricle. The success of mutant identification was in all cases $>95\%$, confirmed by PCR genotyping after selection using previously described sequences for *gnl2* and *ns* (Paridaen et al., 2011) and 5′-agatctgttgacacaaatga-3′ (*gnl3l* gene sequence) paired with the nLTR3 viral sequence 5′-ctgttccatctgttcctgac-3′. Wnt5a control primers are 5′-cagttct-cacgtctgctacttgca-3′ and 5'-acttccggcgtgttggagaattc-3′.

Morpholinos

Injections of embryos at the 1–2 cell stage with morpholinos against p53 (Gene Tools) have been previously described (Langheinrich et al., 2002). After bright field microscopy, the embryos were genotyped to confirm the identity of the mutants.

Northern blots

Total RNA was isolated from embryos (5/sample) using Trizol (Invitrogen). RNA was run on a formaldehyde 1% agarose gel in MOPS buffer and DEPC-treated water for 4 h at 50 V. The gel was soaked in 50 mM NaOH for 15 min followed by 5 min in DEPC-treated water followed by 30 min in 10 × SSC buffer. The RNA was transferred to a positively charged nylon membrane (GE Healthcare) overnight by capillary action and bound to the membrane by UV-crosslinking at 120 mJ. Blots were pre-hybridized for 1 h at

65 °C and subsequently hybridized with DNA probes overnight in ExpressHyb Hybridization Buffer (Clontech) at 65 °C. Probes were made as previously described (Azuma et al., 2006) and labeled with 32P-αCTP (Perkin-Elmer) using a random primer DNA labeling system (Invitrogen). Following hybridization, blots were washed twice for 30 min with 0.1% SDS/0.2 × SSC at 65 °C. Blots were exposed to phospho-imaging screens (Molecular Dynamics) overnight and scanned using a Typhoon Scanner (GE Healthcare). Quantifications here and elsewhere are all tested statistical significance using a Student's two-tailed *t*-test.

Polysome profiling

All steps of this protocol are performed at 4 °C or on ice. Gradients of 17–50% sucrose (11 ml) in gradient buffer (110 mM KAc, 20 mM MgAc and 10 mM HEPES pH 7.6) were poured the evening before use. 25 embryos were lysed in 500 μl polysome lysis buffer (gradient buffer containing 100 mM KCl, 10 mM MgCl, 0.1% NP-40, and freshly added 2 mM DTT and 40 U/ml RNAsin (Promega) using a Dounce tissue grinder (Wheaton). The samples were centrifuged at 1200*g* for 10 min to remove debris and loaded onto the sucrose gradients. The gradients were ultracentrifuged for 2 h at 120,565*g* in an SW41 Ti rotor (Beckman-Coulter, US). The gradients were displaced into a UA6 absorbance reader (Teledyne ISCO) using a syringe pump (Brandel, US) containing 60% sucrose. Absorbance was recorded at an OD of 254 nm. Profiles were performed at least in triplicate, and then were scanned and peak heights were determined using Photoshop CS5 software.

^{35}S- incorporation assay

Per lane, 5 embryos were collected and washed in PBS. Embryos were dissociated by regularly pipetting them up and down in 0.25% trypsin for 10–20 min at 28 °C. The dissociated cells were washed in PBS and incubated in DME medium without methionine or cysteine (Sigma Aldrich) at 28 °C for 30 min. The medium was removed and the cells were incubated in DME containing 20 μCi of ^{35}S-labeled methionine and cysteine (Perkin Elmer) at 28 °C for 30 min. The cells were washed twice in PBS, lysed and run on a 10% SDS/acrylamide gel as described [8]. The gel was fixed in 40% methanol/10% glacial acetic acid for 45 min, washed in water for 20 min and dried in a gel dryer (BioRad) for 2 h at 80 °C. The gels were then exposed to autoradiography film at room temperature.

Acridine orange staining

Live 1 dpf embryos were incubated in E3-embryo medium + 10 μg/mL AO stain (Sigma) in the dark for 30 min. Embryos were washed twice with E3-medium and images were obtained using a Zeiss Axioplan Stereomicroscope (Oberkochen, Germany) equipped with a Leica (Wetzlar, Germany) digital camera using 10 × magnifications. Quantifications were performed by averaging the results of blind counting by 4 individuals of the number of AO positive cells in the tail area beginning where the yolk extension meets the yolk and ending at the tail tip.

Western blots

Western blots were performed as described previously using 5 embryos per lane and a zebrafish-specific p53 antibody (MacInnes et al., 2008). The zebrafish-specific mdm2 antibody was purchased from Anaspec, Fremont CA (#55470), the actin antibody was purchased from Santa Cruz Biotech (sc-1616).

qPCR

Total RNA was isolated using Trizol (Invitrogen) and cDNA was made using iScript (BioRad). qPCR reactions were run using iQ SYBR Green Supermix (BioRad) on a myIQ iCycler (BioRad). The following primers were used: *gnl3l* fw: 5′-acgtgcagtcatgtccaaag-3′, *gnl3l* rv: 5′-gatccttcttccctccatga-3′, *p21* fw: 5′-tgtcaggaaaagcagcagaa-3′, *p21* rv: 5′-ctggtgttttcgggatgttt-3′, *puma* fw: 5′-tcccctccagcttaaggaat-3′, *puma* rv: 5′-atcccagaatcgtgatgtcc-3′, *ef1α* fw: 5′-gagtttgaggctggtatctccaag-3′, *ef1α* rv: 5′-ctcagtggagtccatcttgttgac-3′.

Results

Loss of homologous NS family members results in embryonic lethality

The evolutionary distance between zebrafish *gnl2*, *ns* and *gnl3l* and their homologs in other species is shown in Fig. 1A (the aforementioned genes are boxed in red). By Clustal Omega analysis (http://www.ebi.ac.uk/Tools/msa/clustalo/) of gene sequence homologies, zebrafish *ns* and *gnl3l* are the most closely related (36.5%), while *gnl2* is more distant (26.9% homology to *ns* and 31.9% homology to *gnl3l*). The similarity of the protein domains and their locations in zebrafish Gnl2, Ns, and Gnl3l are also very similar, shown in Fig. 1B, with the 5 GTP-binding domains represented in the middle of all three proteins. Given this high degree of sequence and domain homology between Gnl3l and Gnl2 or Ns, we decided to include gnl3l mutants in our study. We decided to exclude the *gnl1* and *lsg1* genes that are only very distantly related to *ns* and whose protein products are localized in the cytosol (Reynaud et al., 2005). To generate mutant embryos of these proteins, we identified ENU-induced point mutations in the *ns* gene (NM_001002297.1) and *gnl2* gene (NM_213224.1) by TILING, both resulting in early stop codons (Fig. 1B) (Paridaen et al., 2011). The *gnl3l* (NM_001002875.1) mutant was derived by a viral insertion into the first intron of *gnl3l* (Fig. 1B) (Amsterdam et al., 1999). Fig. 1C shows PCR analysis of a single *gnl3l* mutant compared to a wild type sibling using primers that bind the viral insert and the *gnl3l* gene (which would not be expected to amplify any sequence that does not carry the insert in the correct location) along with control primers that amplify the *wnt5a* gene. qPCR analysis using primers spanning the junction between the first two exons was used to verify that the viral insert in the *gnl3l* embryos resulted in an almost complete knockdown of the correctly spliced *gnl3l* transcript (Fig. 1D).

The loss of any ns family member is lethal

Fig. 2 describes in detail the phenotypes of all three mutant embryos during the first 5 days of development. The mutant phenotypes are detectable by morphology at 1 dpf. On this day, mutant embryos appear smaller in head and body size, although these phenotypes are most easily discernable in the *gnl2* and *gnl3l* mutants at this age compared to a subtler phenotype in the ns mutants as previously noted (Paridaen et al., 2011). In addition, at 1 dpf both *gnl2* and *gnl3l* mutants reveal a general apoptotic phenotype (mostly in the head region) including disorganized graying cells and a ragged surface of the skin that is not appreciable in the ns mutants until 2 dpf. Both *gnl2* and *ns* mutants at 1 dpf also display an enlarged forebrain and hindbrain ventricle inflation that, along with the small head and eyes phenotype, are featured in several other ribosome biogenesis mutants (Amsterdam et al., 1999; Chakraborty et al., 2009). Almost all the mutant embryos begin to develop cardiac edemas by 3 dpf, fail to absorb the yolk or inflate the swim bladder, and are dead at the

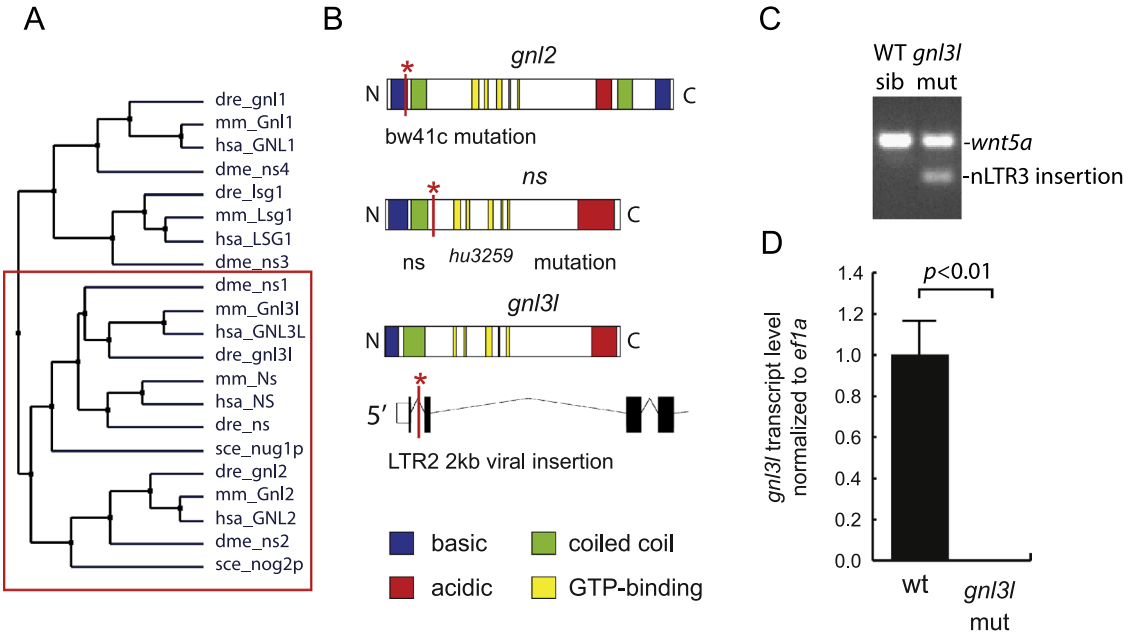

Fig. 1. Overview of the ns family in zebrafish. (A) Representation of the homology between the three family members, and their similarity to homologs in other species. The red box indicates the section of the family tree including ns, gnl2, and gnl3l. This tree was generated using the Blossum algorithm in Jalview (Waterhouse et al., 2009). (B) Graphical representation of the domains of gnl2, ns and gnl3l proteins and part of the gnl3l transcript, respectively showing the location (*) of stop mutations in the bw41c and hu3259 mutants and the location of the viral insert in the hi1437 (gnl3l) mutant used in this study. (C) PCR results using genotyping primers to identify the nLTR3 viral inserts in gnl3l mutants. The *wnt5a* primers are used as controls for the PCR. (D) qPCR analysis of the abundance of correctly spliced *gnl3l* transcript, using primers on both sides of the junction between Exon1 and 2, in wild type and hi1437 embryos. Expression levels were normalized to *ef1α* expression. $p < 0.01$ by Student's two-tailed *t*-test.

end of 5 dpf (Fig. S1). By 5 dpf the phenotypes common in ribosome biogenesis mutants, including the small head and eyes, are particularly evident in the *gnl2* and *ns* mutants, presumably due to a loss of protein synthesis that we show later in Fig. 4C.

Ns family members cleave specific rRNA sites

To examine the effects that the mutation of each zebrafish ns family member has on the processing of rRNA in vertebrates, we performed northern blot analysis of total RNA isolated from each mutant compared to wild type siblings. Fig. 3A illustrates a basic schematic of rRNA processing in zebrafish embryos, derived from previous results (Azuma et al., 2006; Romanova et al., 2009b) and our own observations in this and other studies. In short, pre-rRNA is initially transcribed in a single transcript including the 18S rRNA, 5.8S rRNA, 28S rRNA, the externally transcribed sequence (ETS), and the two internally transcribed sequences (ITS1 and ITS2). This pre-rRNA then undergoes a series of cleavage steps in one of at least two pathways. In Pathway 1, the first nucleotides to be removed are the ETS sequences flanking each side of the transcript, followed by separation of the 18S strand from the 5.8S and 28S strand. In Pathway 2, the first cleavage step separates the 18S from the 5.8S and 28S strand, followed by removal of the ETS sequences. Using probes that bind the ETS, ITS1, ITS2, or 18S rRNA sequence (delineated in Fig. 3A) we were able to detect various impairments of rRNA processing in the mutant embryos compared to their wild type siblings (Fig. 3B). Ratios of band intensities in the mutant lines compared to those of the wild type siblings were determined to estimate the extent of the processing defects (Fig. 3C). In all three mutants, there is an increase of a long rRNA containing the ETS probe sequence, along with a decrease of processing intermediate “d”, suggesting an overall retention of the full-length initial pre-rRNA transcript. Further processing of “d”–“f” is not affected in any of the mutants. The *gnl2* mutant shows a large 2.34 ± 0.15 fold increased retention of the processing intermediates “c” and “e”, which ultimately lead to the mature 5.8S and 28S rRNAs that make up the 60S subunit. In the *ns* and *gnl3l* mutants, a similar defect is observed, but to a far lesser extent. The *ns* mutant shows retention of an additional intermediate, 5.8S rRNA associated with ITS2, labeled “g”. Accumulation of this product is not detected in the other mutants. Given the importance of the 5.8S rRNA in forming the 60S subunit, these results suggest that the *ns* mutants will be especially impaired in their ability to form 60S subunits. The *gnl3l* mutant shows no specific cleavage defects that are not also detected in the other mutants. In all three mutants, a small decrease in the total amount of 18S RNA is observed. These data suggest that both *gnl2* and *ns* have distinctly unique functions regarding the sites of pre-RNA that they cleave. Moreover, given that in both cases the strongest defects are observed in the processing of the 28S rRNA, it would be expected that mutations in *gnl2* and *ns* affect both affect formation of the large 60S ribosomal subunit. In contrast, *gnl3l* appears to have no distinct function in processing rRNA.

Mutant embryos reveal different ribosome biogenesis and protein synthesis defects

To determine the effect of these rRNA processing impairments on the formation of ribosomal subunits and mature ribosomes, we performed polysome profiling on the lysates of mutant embryos compared to their wild type siblings. Representative profiles are shown in Fig. 4A, an overview of all the profiles in this experiment is shown in Fig. S2. We observe that the loss of Gnl2 and Ns results in much more severe impacts on the ribosome profiles compared to the loss of Gnl3l. A reduction of the 80S peak is seen in all three of the mutants, although the most significant reductions are observed in the *gnl2* and *ns* mutants (Fig. 4A,B). Strikingly, an almost complete collapse of the 60S peak is seen in the ns mutants, which is not observed in the *gnl2* or *gnl3l* mutants (Fig. 4A,B). Moreover, consistent with the results in Fig. 3

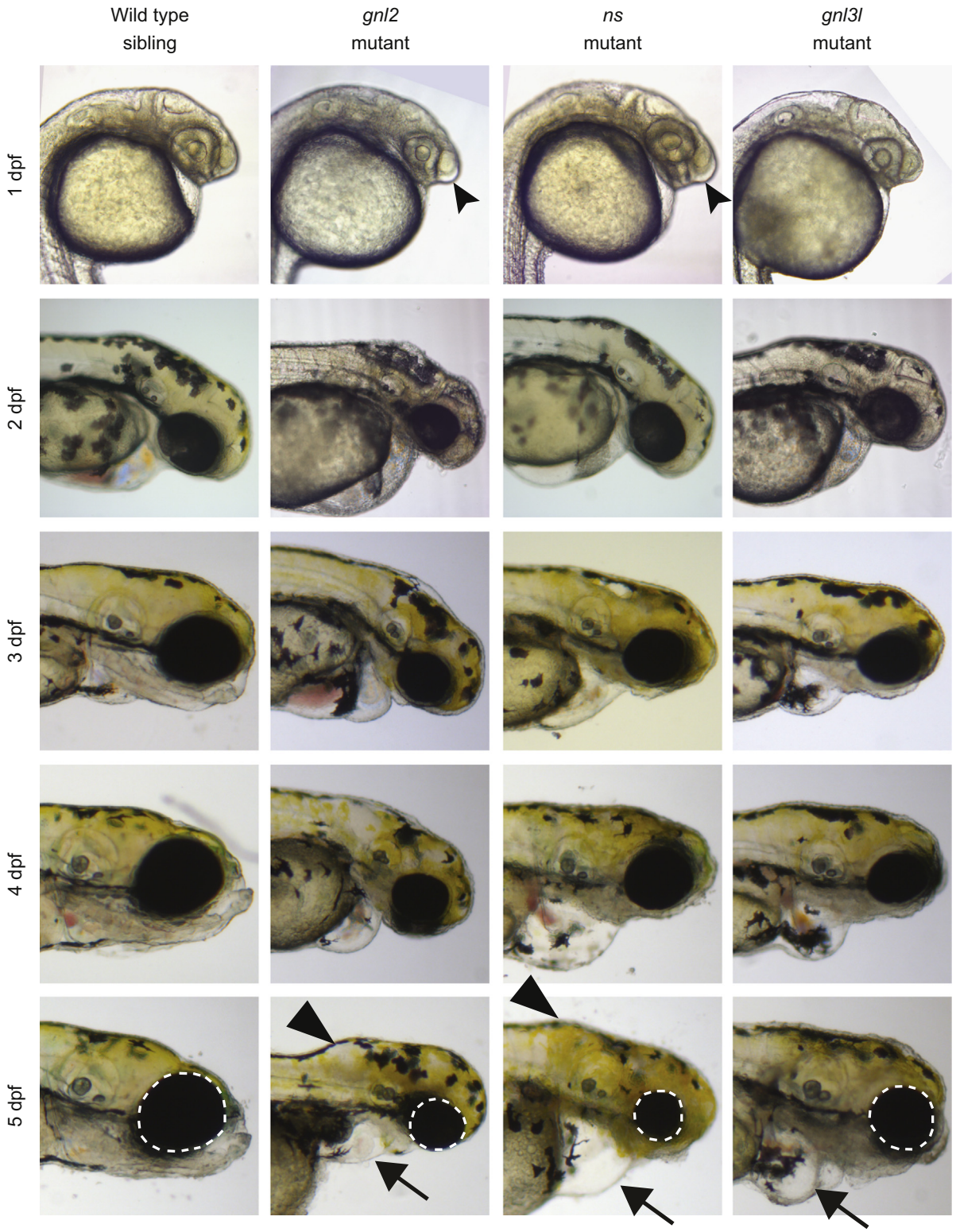

Fig. 2. Morphology of ns family member mutants. Bright-field microscopy showing the morphological phenotypes of the mutants compared to a wild type sibling of gnl2 (there was no appreciable difference between wild type siblings of ns, gnl2, or gnl3l, therefore only gnl2 wild type siblings are shown for space reasons). The enlargement of the forebrain at 1 dpf is depicted with forked arrowheads. The inflation of the hindbrain ventricle is depicted at 5 dpf with arrowheads, and the cardiac edemas depicted with arrows. The size of the eyes at 5 dpf is illustrated with the white dotted circles.

suggesting impairment of 60S subunits, we observe the presence of halfmers in both *gnl2* and *ns* mutant profiles, which correspond to an increase of mRNAs that are only bound to the 40S small subunit (Pisarev et al., 2008). We do not detect a decrease of the 60S peak in the *gnl2* mutant profiles, but the 80S peak is more strongly decreased than in the *ns* mutant profiles, suggesting that the 60S ribosomal subunits are present in normal amounts in the *gnl2* mutants, albeit impaired in such a way as to prevent proper association with the 40S subunit. We showed previously that the loss of both *ns* and *gnl2* results in a synergistic worsening of the

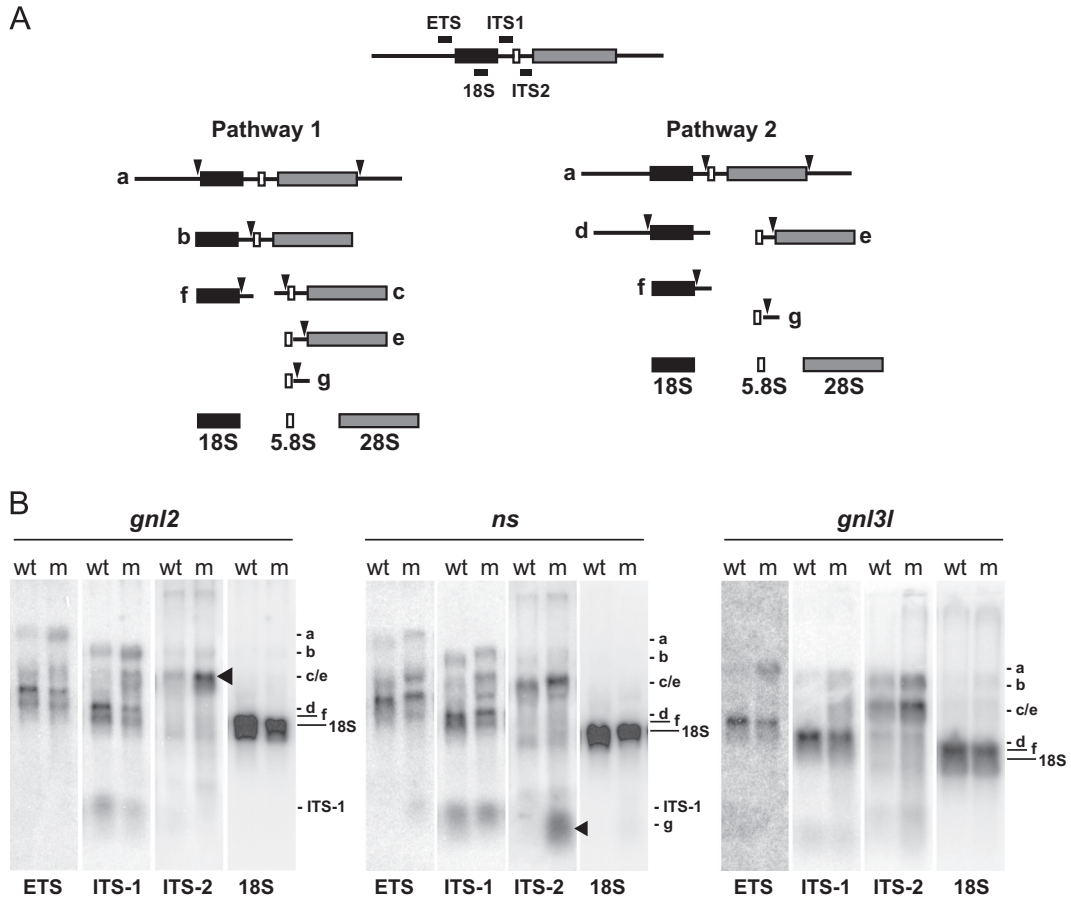

C

Relative band intensity compared to sibling

blot	step	gnl2	ns	gnl3l
ETS	a→d	0.64±0.27	0.308±0.095	0.3±0.18
ITS1	b→c/e	1.54±0.12	1.62±0.84	1.47±0.31
ITS1	d→f	0.990±0.013	0.993±0.079	0.97±0.15
ITS2	ce	2.34±0.15	1.37±0.37	1.332±0.083
18S	18S	0.831±0.013	0.95±0.11	0.85±0.11

Fig. 3. Specific rRNA processing defects are evident in ns and gnl2 mutants. (A) Simplified schematic of rRNA processing. The locations of the probes used and the processing intermediates visualized in (B) are indicated. (B) Northern blots showing reduced cleavage activity in various rRNA processing steps in gnl2, ns and gnl3l mutants at 2 dpf. The arrowheads indicate sites of major processing defects in the mutants. Results are representative of at least three independent experiments. (C) Relative band intensities were measured using ImageJ software and are represented relative to the wild type sibling for each mutant. $p < 0.01$ by Student's two-tailed *t*-test.

morphological phenotypes described in Fig. 2 (Paridaen et al., 2011). Likewise, when we injected *ns* mutant embryos with morpholinos that block the translation of *gnl2* mRNA we observe a dramatic decrease of the 80S peak and polysome numbers in the profiles, reinforcing the notion that both proteins function distinctly in ribosome biogenesis (Fig. S3). The *gnl3l* mutant profiles are also consistent with the northern blot results in Fig. 3, in that there appears to be a minor reduction of the overall number of monosomes and polysomes, but no specific defects are visible. To confirm that alterations in the polysome profile are not a common result of embryonic lethal mutations, we performed polysome profiling on embryos with an unrelated lethal mutation in the cilia gene *lccr50*. As expected, loss of *lccr50* had no effect on polysome profiles (Fig. S2).

To determine how the observed defects in rRNA processing and 60S ribosomal subunit formation in the *ns* and *gnl2* mutants affect protein synthesis compared to the *gnl3l* mutants, we labeled mutant embryonic cells with ^{35}S-methionine for 30 min and compared the total amount of protein produced to their wild type siblings. Both *ns* and *gnl2* mutant cells show a significant reduction of the amount of total protein synthesized in the 30-minute pulse (Fig. 4C,D). Surprisingly, no difference was observed in the *gnl3l* mutant cells (Fig. 4C,D). These results for *ns* and *gnl2* correspond as would be expected with the polysome profile results, and also suggest that despite the minor reduction of peak sizes in the profiles of the *gnl3l* mutants that this is not sufficient to impair protein synthesis.

Loss of all ns family members induces p53 stabilization and apoptosis

In order to determine whether the differences in ribosome formation and protein synthesis we observe in the *gnl3l* compared

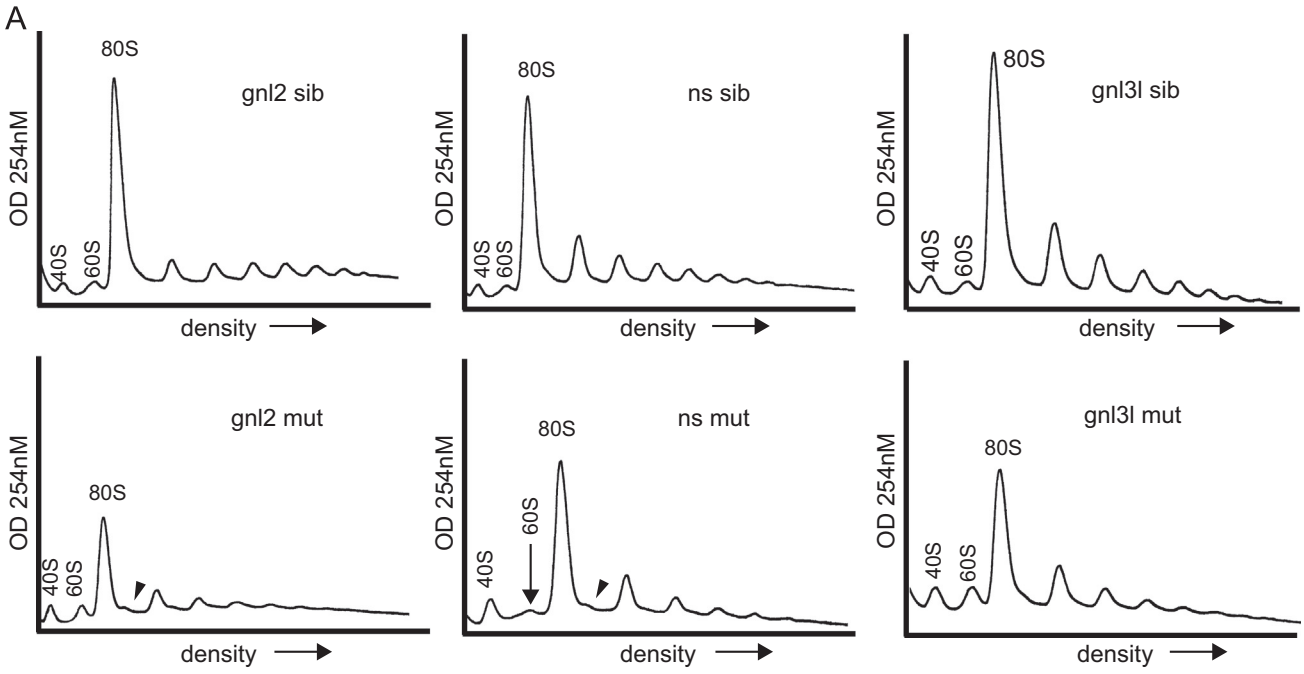

B

	Mutant 80S peak/ Wild type sib 80S peak			Mutant 60S peak/ Mutant 40S peak		
	ratio	STD	*p*-value	ratio	STD	*p*-value
gnl2	0.543	0.106	0.003	0.849	0.307	NS
ns	0.585	0.218	0.036	0.368	0.089	0.003
gnl3l	0.615	0.117	0.001	1.123	0.499	NS

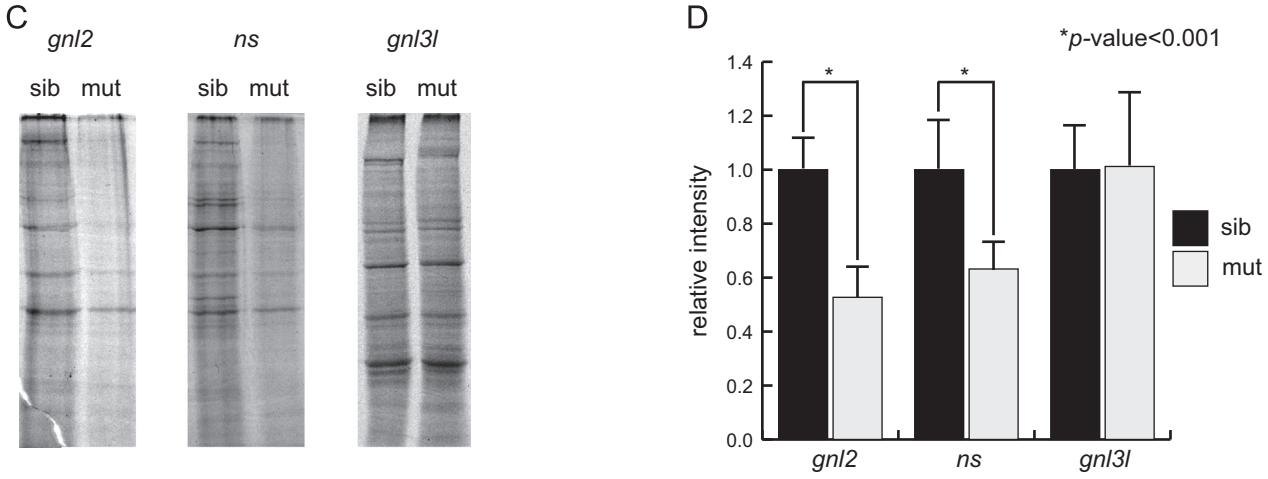

Fig. 4. Polysome profiles reveal different effects of the mutations on ribosome biogenesis. (A) Polysome profiles of gnl2, ns and gnl3l mutants at 2 dpf. Location of the small (40S) and large (60S) subunits, as well as the monosome (80S) and halfmers (arrowheads) are indicated. The arrow indicates the collapsed 60S peak in the ns mutants. Results are representative of at least three independent experiments (shown in Fig. S1). (B) Quantification of peak sizes including profiles in Fig. S1. The ratios of the size of the mutant 80S peak to the wild type sibling 80S peak are shown on the left. The ratio of the mutant 60S peaks to the mutant 40S peaks are shown on the right. STD=standard deviation, NS=not significant. (C) Representative exposures of ^{35}S-radiolabeled total protein synthesized in a 30-minute pulse in embryonic cells. (D) Quantifications of whole lane intensity in at least 3 samples (11 samples for gnl3l experiments). $p < 0.01$ by Student's two-tailed *t*-test.

to *ns* and *gnl2* mutants results in a corresponding reduction of p53 stabilization, we measured the level of apoptosis and p53 stabilization in all the mutants compared to their wild-type siblings. Despite the relatively unaffected levels of ribosome biogenesis and normal levels of protein synthesis in the *gnl3l* mutants, we found that apoptosis measured by acridine orange staining is in fact significantly increased in the *gnl3l* mutants to similar levels as we expected to observe in the *gnl2* and *ns* mutants (Fig. 5A,B).

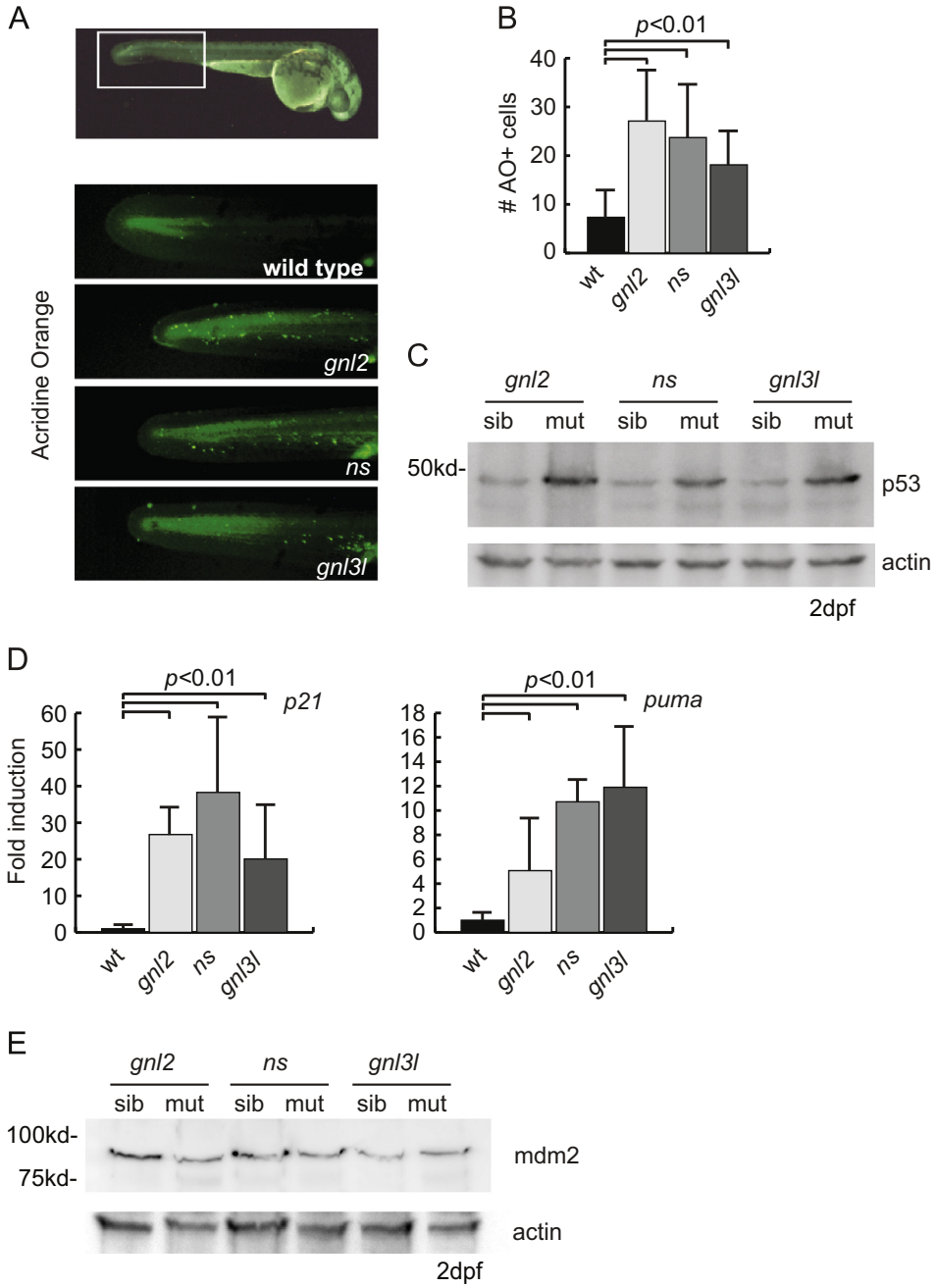

Fig. 5. p53 induced apoptosis in ns family mutants. (A) Representative fluorescent microscopy images showing acridine orange staining at 1 dpf. The top box illustrates with the white box the portion of the tail used for quantification of acridine orange positive cells. (B) Quantifications of the number of acridine orange positive cells. At least 7 animals were blindly scored for these quantifications. $p < 0.01$ by Student's two-tailed *t*-test. (C) Western blot analysis of p53 stabilization in all three mutant lines at 2 dpf. (D) qPCR analysis of *p21* and *puma* transcript levels at 2 dpf, normalized to *ef1α* expression. $p < 0.01$ by Student's two-tailed *t*-test. (E) Western blot analysis of zebrafish mdm2 levels in mutants and wild type siblings at 2 dpf.

Correspondingly, western blot analysis reveals all three of the mutant lines stabilize p53 to a similar degree (Fig. 5C). p53 stabilization in all three mutant lines additionally leads to transcription of the p53 target genes *p21* and *puma*, associated with the induction of senescence and apoptosis respectively (Fig. 5D).

A major negative regulator of the p53 tumor suppressor is the MDM2 protein, which in normal cells keeps p53 at low expression levels via constitutive ubiquitination and degradation (Momand et al., 1992). Since NS and GNL3L have both been shown in human cell lines to have roles destabilizing or stabilizing MDM2, respectively (Meng et al., 2011a, 2008), we determined what the effects were of the loss of zebrafish *gnl2*, *ns*, and *gnl3l* on the stability of Mdm2. Fig. 5E shows western blot analysis with a zebrafish-specific Mdm2 antibody indicating that the loss of none of the ns family member proteins in this model results in any appreciable difference in the levels of endogenous Mdm2.

Loss of p53 partially rescues mutant phenotypes

Morpholinos (MO) designed to deplete zebrafish embryos of p53 have been previously described (Langheinrich et al., 2002). The injection of mutant embryos with the p53 MO results in a partial rescue of the morphological phenotypes, including the small head and eyes phenotypes (Fig. 6A). Specifically in the *ns*

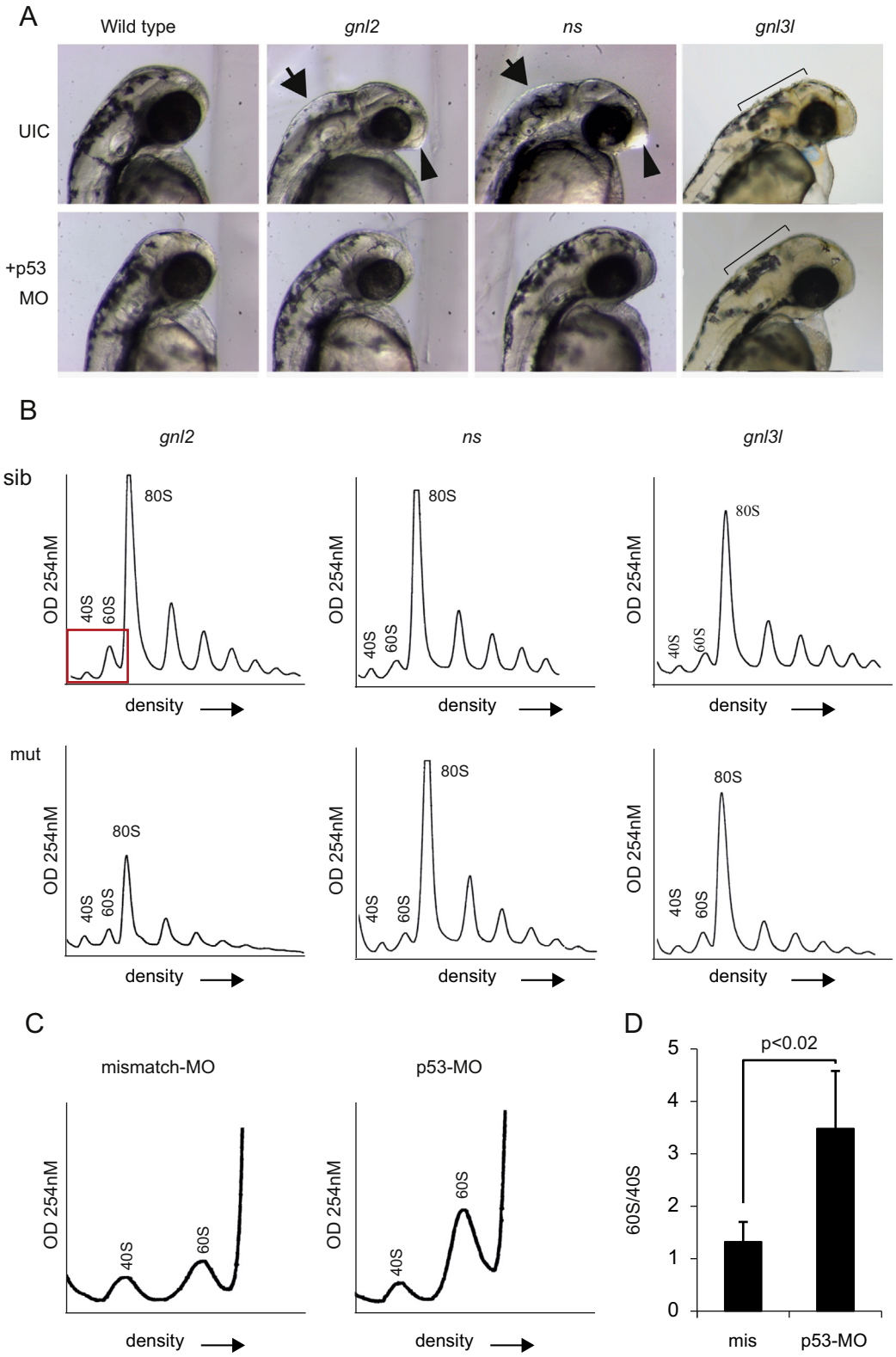

Fig. 6. Loss of p53 partially rescues mutant phenotypes. (A) Bright field microscopy of p53 MO injections at 2 dpf. UIC = uninjected control embryos. Arrows depict inflation of the hindbrain ventricle, arrowheads depict enlargement of the forebrain. The ragged skin phenotype in gnl3l mutants and the rescue are depicted with the black bars. (B) Representative profiles of mutant embryos injected with the p53 MO. (C) Magnified representation of polysome profiles showing an increase in 60S peak size in p53 MO compared to missense MO injected embryos. (D) Quantification of the ratio of 60S to 40S peak size in missense vs. p53 MO injected embryos.

and *gnl2* mutants a rescue effect is observed in the inflation of the hindbrain ventricle and enlarged forebrain, while in the *gnl3l* mutants a smoothing of the ragged skin phenotype is seen (Fig. 6A). We then profiled the mutant embryos injected with the p53 MO. We first injected mutant embryos with missense MOs and found that all the profiles looked identical to those presented in Fig. 4A (data not shown). When we injected the p53 MO into the mutant embryos we observed an increase of the peak sizes in all

the mutants (Fig. 6B, additional profiles are shown in Fig S4). This is particularly striking in the *ns* mutants, where the collapse of the 60S subunit appears to be completely restored and the monosomal as well as the polysomal peaks are substantially higher. This increase of peak sizes in the mutants is likely due to the effect of the p53 MO in general to increase the amount 60S subunits, since in all our wild type sibling control injections we also observed an increase of 60S and 80S peak sizes (Fig. 6B). This is shown in detail in Fig. 6C where we compared the 40S and 60S peaks of wild type sibling embryos injected with the missense MO compared to the p53 MO. The size ratio of the 60S peak to the 40S peak in the missense MO injected embryos compared to the p53 MO is quantified in Fig. 6D, indicating that the p53 MO clearly has an unexpected effect of increasing the number of 60S ribosomal subunits.

Discussion

This work provides a detailed analysis of how the Ns family members function in vertebrate ribosome biogenesis and protein synthesis, the most important finding being that Gnl3l does not function as expected in these contexts at all. This result was surprising, given the high sequence and protein domain homology of Gnl3l to the Ns and Gnl2 proteins, both with critical functions in ribosome biogenesis and protein production that we describe in depth in this work. Since the loss of Gnl3l in zebrafish is equally lethal as the loss of Ns or Gnl2, it is clear that Gnl3l has functions unrelated to ribosome biogenesis that are nonetheless critical for development.

Our results suggest that in the *ns* mutants, the failure of the 5.8S rRNA sequence (an integral component of the large 60S ribosomal subunit) to be cleaved from the ITS2 sequence may be the cause of the unique collapse of the 60S subunit we observe in the polysome profiles of Fig. 4A. Interestingly, pre-5.8S rRNA in *S. cerevisiae* has been shown to co-precipitate with Lsg1, a more distant family member of NS (see Fig. 1A), suggesting a conserved function of 5.8S rRNA processing between the two proteins. As mentioned in the introduction, NS is able to shuttle from the nucleoplasm to the nucleolus depending on the binding of GTP (Tsai and McKay, 2005). It seems likely then that NS is functioning to shuttle other nuclear proteins into the nucleolus that are required for pre-RNA processing. One potential protein that could fit this role is the NOP2 protein, which has been previously shown by a large-scale quantitative tandem mass spectrometry analysis of cell fractions to complex with NS (Havugimana et al., 2012). NOP2 is also known to localize to both the nucleus and nucleoplasm, and the loss of NOP2 has been demonstrated to cause pre-RNA processing defects including impaired maturation of the 5.8S rRNA and collapse of the 60S ribosomal subunit (de Beus et al., 1994; Hong et al., 1997). Interestingly, the expression of NOP2 in cells also increases in states of high growth and decreases in stationary phases, similar to the expression of NS (de Beus et al., 1994; Tsai and McKay, 2002). Taken together, these studies and our data suggest that a major role of NS is to shuttle rRNA processing proteins, such as NOP2 (although other proteins are likely involved), into the nucleolus from the nucleus during pre-differentiated states of high cell growth requiring robust levels of ribosome biogenesis in order to function in the processing of 5.8S rRNA that will ultimately assemble the large 60S ribosomal subunit. While a complete description of the interactions between NS and NOP2 are presently beyond the scope of this manuscript, we hope this analysis will provide a cogent platform for future studies of NS function.

Given the marked rRNA processing delays revealed in the *gnl2* mutants, we were surprised to see very little difference in the total numbers of 40S and 60S subunits on the profiles. However, it is clear that despite this insignificant reduction, the loss of Gnl2 has a major effect on the ability of the 60S subunit to bind the 40S subunit, accounting for the decrease of the 80S monosome peak, the appearance of halfmers, and the subsequent reduction of total protein synthesis. While at this point we may only speculate upon the nature of this impairment, possibly Gnl2 has a second role in the export of the 60S subunit to the cytoplasm in a manner reminiscent of another function of Lsg1 besides 5.8S rRNA maturation. Studies in *S. cerevisiae* and more recently in *Drosophila* have shown that the GTPase domain of Lsg1 is required for release of the nuclear export signal (NES)-bearing protein Nmd3 from cytoplasmic 60S subunits, and that mutations reducing GTPase activity of Lsg1 result in the nucleolar retention of 60S subunits (Hartl et al., 2013; Kallstrom et al., 2003). Therefore while the loss of Gnl2 may slow the production of 60S subunits due to rRNA impairments as we show in Fig. 3B, a potential retention and accumulation of immature 60S subunits in the nucleolus may represent the unchanged 60S peak size we see in Fig. 4A, and also explain the decrease of the 80S monosomal peak.

Previous reports have suggested that the mechanism for p53 stabilization upon the depletion of NS in mammalian cells involves the nucleolar release of ribosomal proteins RPL5 and RPL11 and the subsequent binding of these proteins with MDM2, the negative regulator of p53 (Dai et al., 2008). Recently it was revealed that impaired ribosome biogenesis in fact results in a complex containing RPL5, RPL11, and 5S rRNA being redirected to HDM2 (human MDM2) instead of nascent 60S subunits, suggesting this may also be occurring in the ns mutants (Donati et al., 2013). Our results regarding the collapse of the 60S ribosomal subunit, where RPL5 and RPL11 normally reside, upon the loss of ns in zebrafish are consistent with this mechanism. However, our data suggest that this is not what is occurring with the loss of Gnl2 or Gnl3l3, neither of which results in a decrease of 60S subunits (suggesting RPL5 and RPL11 are maintained in the subunit). Attempts to perform co-immunoprecipitation assays with RPL11 or RPL5 and MDM2 antibodies with lysates from zebrafish embryos were not successful, we are therefore unable to state for certain that the loss of any ns family member in zebrafish embryos results in the endogenous interaction between these proteins. The mechanism of p53 stabilization in the *gnl3l* mutants is even more mysterious, given how there is no ribosome biogenesis or protein production phenotype upon its loss. While there are reports that the reduction of GNL3L in human cell lines destabilizes MDM2 and leads to p53 stabilization (Meng et al., 2011a), our results indicate that the levels of endogenous Mdm2 in zebrafish remain unchanged upon the loss of gnl3l. Other studies have shown a function of human GNL3L in the transition of metaphase-to-anaphase through the stabilization of the telomere-capping protein TRF1 (part of the chromosome-protective shelterin complex), and demonstrate that GNL3L overexpression leads to shortening of the telomeres (Fu and Collins, 2007). It may be then that a reduction of GNL3L destabilizes TRF1 and results in improper telomere lengthening. Such lengthening has been shown in *S. cerevisae* to activate the checkpoint protein Rad53, the homolog of human CHK2, and cause cell cycle arrest (Viscardi et al., 2003). Since CHK2 in vertebrate cells is a well-known upstream mediator of the p53 pathway (Chehab et al., 2000), future studies on p53 stabilization from the loss of GNL3L may be more appropriately focused on the role of GNL3L in the protection of telomere ends rather than a role in ribosome biogenesis.

The remarkable rescue effect of the p53 MO on the peak sizes of the *ns* polysomes profiles was unexpected, however it is clear that the loss of p53 has a general effect on increasing the number of 60S subunits. This may be relevant in the context of studies demonstrating that the RPL5/RPL11/5S rRNA complex has an

important role in stabilizing p53 through inhibition of HDM2 (Donati et al., 2013). Here the authors propose that in a model of hyperactivated ribosome biogenesis (such as embryonic development) excessive amounts of the RPL5/RPL11/5S rRNA complex may instead inhibit HDM2 rather than being incorporated into 60S subunits. Presumably in such a case p53 is used as a checkpoint to prevent uncontrolled levels of translation. Thus in the absence of p53, cells containing unusually high numbers of 60S subunits would not undergo apoptosis per usual. While the physiological relevance of this observation is not clear (p53 MO injected embryos have no obvious phenotypes unless challenged with DNA damage (Langheinrich et al., 2002)) this is nonetheless a very interesting observation that is certainly worthy of future study.

The increasing importance of NS is underscored by the large amount of attention it has been receiving lately in the fields of stem cells, cancer cells, and tissue regeneration. The potential clinical relevance of NS is demonstrated by the recent observation that inhibiting NS in cancer cells results in cell cycle arrest regardless of the status of the p53 tumor suppressor (Liu et al., 2010). We show in this report that despite their large degree of sequence and domain homology, the NS family members in vertebrates function in unexpectedly different roles. These results will hopefully increase understanding about the specific cellular functions of each NS family member in a way that is useful to those in the fields of stem cells, cancer, and tissue regeneration. Moreover, we envision this work will be beneficial for the current efforts underway to target NS in cancer cells, as well as for future work that may include the targeting GNL2 and GNL3L.

Appendix A. Supporting information

Supplementary data associated with this article can be found in the online version at http://dx.doi.org/10.1016/j.ydbio.2013.10.029.

References

Amsterdam, A., Burgess, S., Golling, G., Chen, W., Sun, Z., Townsend, K., Farrington, S., Haldi, M., Hopkins, N., 1999. A large-scale insertional mutagenesis screen in zebrafish. Genes Dev. 13, 2713–2724.

Azuma, M., Toyama, R., Laver, E., Dawid, I.B., 2006. Perturbation of rRNA synthesis in the bap28 mutation leads to apoptosis mediated by p53 in the zebrafish central nervous system. J. Biol. Chem. 281, 13309–13316.

Beekman, C., Nichane, M., De Clercq, S., Maetens, M., Floss, T., Wurst, W., Bellefroid, E., Marine, J.C., 2006a. Evolutionarily conserved role of nucleostemin: controlling proliferation of stem/progenitor cells during early vertebrate development. Mol. Cell Biol. 26, 9291–9301.

Beekman, C., Nichane, M., De Clercq, S., Maetens, M., Floss, T., Wurst, W., Bellefroid, E., Marine, J.C., 2006b. Evolutionarily conserved role of nucleostemin: controlling proliferation of stem/progenitor cells during early vertebrate development. Mol. Cell Biol. 26, 9291–9301.

Chakraborty, A., Uechi, T., Higa, S., Torihara, H., Kenmochi, N., 2009. Loss of ribosomal protein L11 affects zebrafish embryonic development through a p53-dependent apoptotic response. PloS One 4, e4152.

Chehab, N.H., Malikzay, A., Appel, M., Halazonetis, T.D., 2000. Chk2/hCds1 functions as a DNA damage checkpoint in G(1) by stabilizing p53. Genes Dev. 14, 278–288.

Dai, M.S., Sun, X.X., Lu, H., 2008. Aberrant expression of nucleostemin activates p53 and induces cell cycle arrest via inhibition of MDM2. Mol. Cell Biol. 28, 4365–4376.

de Beus, E., Brockenbrough, J.S., Hong, B., Aris, J.P., 1994. Yeast NOP2 encodes an essential nucleolar protein with homology to a human proliferation marker. J. Cell Biol. 127, 1799–1813.

Donati, G., Peddigari, S., Mercer, C.A., Thomas, G., 2013. 5S Ribosomal RNA is an essential component of a nascent ribosomal precursor complex that regulates the Hdm2-p53 checkpoint. Cell Rep. 4, 87–98.

Fu, D., Collins, K., 2007. Purification of human telomerase complexes identifies factors involved in telomerase biogenesis and telomere length regulation. Mol. Cell 28, 773–785.

Golling, G., Amsterdam, A., Sun, Z., Antonelli, M., Maldonado, E., Chen, W., Burgess, S., Haldi, M., Artzt, K., Farrington, S., Lin, S.Y., Nissen, R.M., Hopkins, N., 2002. Insertional mutagenesis in zebrafish rapidly identifies genes essential for early vertebrate development. Nat. Genet. 31, 135–140.

Hartl, T.A., Ni, J., Cao, J., Suyama, K.L., Patchett, S., Bussiere, C., Gui, D.Y., Tang, S., Kaplan, D.D., Fish, M., Johnson, A.W., Scott, M.P., 2013. Regulation of ribosome biogenesis by nucleostemin 3 promotes local and systemic growth in Drosophila. Genetics 194, 101–115.

Havugimana, P.C., Hart, G.T., Nepusz, T., Yang, H., Turinsky, A.L., Li, Z., Wang, P.I., Boutz, D.R., Fong, V., Phanse, S., Babu, M., Craig, S.A., Hu, P., Wan, C., Vlasblom, J., Dar, V.U., Bezginov, A., Clark, G.W., Wu, G.C., Wodak, S.J., Tillier, E.R., Paccanaro, A., Marcotte, E.M., Emili, A., 2012. A census of human soluble protein complexes. Cell 150, 1068–1081.

Hong, B., Brockenbrough, J.S., Wu, P., Aris, J.P., 1997. Nop2p is required for pre-rRNA processing and 60S ribosome subunit synthesis in yeast. Mol. Cell Biol. 17, 378–388.

Kallstrom, G., Hedges, J., Johnson, A., 2003. The putative GTPases Nog1p and Lsg1p are required for 60S ribosomal subunit biogenesis and are localized to the nucleus and cytoplasm, respectively. Mol. Cell Biol. 23, 4344–4355.

Langheinrich, U., Hennen, E., Stott, G., Vacun, G., 2002. Zebrafish as a model organism for the identification and characterization of drugs and genes affecting p53 signaling. Curr. Biol.: CB 12, 2023–2028.

Liu, R., Zhang, Z., Xu, Y., 2010. Downregulation of nucleostemin causes G1 cell cycle arrest via a p53-independent pathway in prostate cancer PC-3 cells. Urol. Int. 85, 221–227.

Ma, H., Pederson, T., 2007. Depletion of the nucleolar protein nucleostemin causes G1 cell cycle arrest via the p53 pathway. Mol. Biol. Cell 18, 2630–2635.

MacInnes, A.W., Amsterdam, A., Whittaker, C.A., Hopkins, N., Lees, J.A., 2008. Loss of p53 synthesis in zebrafish tumors with ribosomal protein gene mutations. Proc. Natl. Acad. Sci. USA 105, 10408–10413.

Maki, N., Takechi, K., Sano, S., Tarui, H., Sasai, Y., Agata, K., 2007. Rapid accumulation of nucleostemin in nucleolus during newt regeneration. Dev. Dyn.: Off. Publ. Am. Assoc. Anat. 236, 941–950.

Meng, L., Hsu, J.K., Tsai, R.Y., 2011a. GNL3L depletion destabilizes MDM2 and induces p53-dependent G2/M arrest. Oncogene 30, 1716–1726.

Meng, L., Hsu, J.K., Zhu, Q., Lin, T., Tsai, R.Y., 2011b. Nucleostemin inhibits TRF1 dimerization and shortens its dynamic association with the telomere. J. Cell Sci. 124, 3706–3714.

Meng, L., Lin, T., Tsai, R.Y., 2008. Nucleoplasmic mobilization of nucleostemin stabilizes MDM2 and promotes G2-M progression and cell survival. J. Cell Sci. 121, 4037–4046.

Meng, L., Yasumoto, H., Tsai, R.Y., 2006. Multiple controls regulate nucleostemin partitioning between nucleolus and nucleoplasm. J. Cell Sci. 119, 5124–5136.

Meng, L., Zhu, Q., Tsai, R.Y., 2007. Nucleolar trafficking of nucleostemin family proteins: common versus protein-specific mechanisms. Mol. Cell Biol. 27, 8670–8682.

Momand, J., Zambetti, G.P., Olson, D.C., George, D., Levine, A.J., 1992. The mdm-2 oncogene product forms a complex with the p53 protein and inhibits p53-mediated transactivation. Cell 69, 1237–1245.

Ohmura, M., Naka, K., Hoshii, T., Muraguchi, T., Shugo, H., Tamase, A., Uema, N., Ooshio, T., Arai, F., Takubo, K., Nagamatsu, G., Hamaguchi, I., Takagi, M., Ishihara, M., Sakurada, K., Miyaji, H., Suda, T., Hirao, A., 2008. Identification of stem cells during prepubertal spermatogenesis via monitoring of nucleostemin promoter activity. Stem Cells 26, 3237–3246.

Paridaen, J.T., Janson, E., Utami, K.H., Pereboom, T.C., Essers, P.B., van Rooijen, C., Zivkovic, D., Macinnes, A.W., 2011. The nucleolar GTP-binding proteins Gnl2 and nucleostemin are required for retinal neurogenesis in developing zebrafish. Dev. Biol. 355, 286–301.

Pisarev, A.V., Kolupaeva, V.G., Yusupov, M.M., Hellen, C.U., Pestova, T.V., 2008. Ribosomal position and contacts of mRNA in eukaryotic translation initiation complexes. EMBO J. 27, 1609–1621.

Qu, J., Bishop, J.M., 2012. Nucleostemin maintains self-renewal of embryonic stem cells and promotes reprogramming of somatic cells to pluripotency. J. Cell Biol. 197, 731–745.

Rao, M.R., Kumari, G., Balasundaram, D., Sankaranarayanan, R., Mahalingam, S., 2006. A novel lysine-rich domain and GTP binding motifs regulate the nucleolar retention of human guanine nucleotide binding protein, GNL3L. J. Mol. Biol. 364, 637–654.

Reynaud, E.G., Andrade, M.A., Bonneau, F., Ly, T.B., Knop, M., Scheffzek, K., Pepperkok, R., 2005. Human Lsg1 defines a family of essential GTPases that correlates with the evolution of compartmentalization. BMC Biol. 3, 21.

Romanova, L., Grand, A., Zhang, L., Rayner, S., Katoku-Kikyo, N., Kellner, S., Kikyo, N., 2009a. Critical role of nucleostemin in pre-rRNA processing. J. Biol. Chem. 284, 4968–4977.

Romanova, L., Grand, A., Zhang, L., Rayner, S., Katoku-Kikyo, N., Kellner, S., Kikyo, N., 2009b. Critical role of nucleostemin in pre-rRNA processing. J. Biol. Chem. 284, 4968–4977.

Rosby, R., Cui, Z., Rogers, E., de Livron, M.A., Robinson, V.L., DiMario, P.J., 2009. Knockdown of the Drosophila GTPase nucleostemin 1 impairs large ribosomal subunit biogenesis, cell growth, and midgut precursor cell maintenance. Mol. Biol. Cell 20, 4424–4434.

Shugo, H., Ooshio, T., Naito, M., Naka, K., Hoshii, T., Tadokoro, Y., Muraguchi, T., Tamase, A., Uema, N., Yamashita, T., Nakamoto, Y., Suda, T., Kaneko, S., Hirao, A., 2012. Nucleostemin in injury-induced liver regeneration. Stem Cells Dev. 21, 3044–3054.

Thisse, B., Thisse, C., 2004. Fast release clones: a high throughput expression analysis. ZFIN Dir. Data Submiss. ⟨http://zfin.org⟩.

Tsai, R.Y., McKay, R.D., 2002. A nucleolar mechanism controlling cell proliferation in stem cells and cancer cells. Genes Dev. 16, 2991–3003.

Tsai, R.Y., McKay, R.D., 2005. A multistep, GTP-driven mechanism controlling the dynamic cycling of nucleostemin. J. Cell Biol. 168, 179–184.

Viscardi, V., Baroni, E., Romano, M., Lucchini, G., Longhese, M.P., 2003. Sudden telomere lengthening triggers a Rad53-dependent checkpoint in *Saccharomyces cerevisiae*. Mol. Biol. Cell 14, 3126–3143.
Waterhouse, A.M., Procter, J.B., Martin, D.M., Clamp, M., Barton, G.J., 2009. Jalview Version 2—a multiple sequence alignment editor and analysis workbench. Bioinformatics 25, 1189–1191.
Westerfield, M., 1995. The Zebrafish Book: A Guide for the Laboratory use of Zebrafish (Brachydanio rerio). University of Oregon Press, Eugene, OR.
Wienholds, E., Plasterk, R.H., 2004. Target-selected gene inactivation in zebrafish. Methods Cell Biol. 77, 69–90.
Yasumoto, H., Meng, L., Lin, T., Zhu, Q., Tsai, R.Y., 2007. GNL3L inhibits activity of estrogen-related receptor gamma by competing for coactivator binding. J. Cell Sci. 120, 2532–2543.